ISSN 1063-7834, Physics of the Solid State, 2020, Vol. 62, No. 10, pp. 1815–1829. © Pleiades Publishing, Ltd., 2020.

SEMICONDUCTORS

Pressure Effect Study on the Electronic and Optical Properties of $B_xIn_{1-x}As$ Alloys Using DFT Calculation

M. Guemou[a, *], M. Khelil[a], and A. Abdiche[b]

[a] *Department of Sciences and Technologies, University of Tiaret, Tiaret, Algeria*
[b] *Electrical Engineering Department, Faculty of Applied Sciences, University of Tiaret, Tiaret, Algeria*
** e-mail: guemoumhamed7@gmail.com*

Received May 20, 2020; revised June 4, 2020; accepted June 5, 2020

Abstract—In order to extract structural and electronic properties of $B_xIn_{1-x}As$ ternary alloys and enrich the database of materials based on boron and indium, we have used full-potential augmented plane wave (FP-LAPW) method through the density function theory (DFT) and within generalized gradient approximation (GGA), local density approximation (LDA), and Tran–Blaha modified Becke–Johnson approximation (TB–mBJ). We have optimized the cohesive energy of our binary compound and ternary alloys versus volume of the unit cell firstly, and we have found that the optimum volume, lattice parameter, and the bulk modulus vary for different boron concentrations. Using DFT–mBJ calculations, we found that InAs possess direct band-gap energy and an indirect gap semiconductor for BAs and $B_{0.75}In_{0.25}As$. However, $B_{0.25}In_{0.75}As$ and $B_{0.5}In_{0.5}As$ ternary alloys have a metallic and semi metallic characters, respectively. We also studied the optical properties of our BAs and InAs binary and $B_{0.75}In_{0.25}As$ ternary semiconductors and their behaviors are also investigated under the application of hydrostatic pressure in a range of 0 to 25 GPa. In summary, we conclude that the incorporation of boron atom in InAs increase its hardness and affects the band-gap energy considerably, and therefore provides a novel research perspective. We note that InAs binary compound loses its semiconductor character and becomes semi-metal at 5 GPa.

Keywords: InAs, BAs, $B_xIn_{1-x}As$, mBJ approximation

DOI: 10.1134/S106378342010011X

1. INTRODUCTION

Researchers were found compelled to meet the increasing requirements of companies and enterprises in different field, in the recent few years. Study, characterize, analyze, predict, and develop new materials for new applications are the most important preoccupation of laboratories by means of theoretical and experimental works.

In the parallel with the progress made in technology and growing techniques of semiconductors, researchers are invited to follow this evolution and must devote many works to predict new materials with structural and electronic properties that can enhance the quality of various devices.

Semiconductor materials containing the atom of indium (In) or that of arsenic (As) find an important place in current research [1–5], for their attractive properties in many applications [6–9].

Among this group, InAs and BAs have different structural and electronic properties that we can combine in ternary alloy $B_xIn_{1-x}As$, with the objective to obtain new materials with controllable properties. These will serve as another alternative for optoelectronic devices and extend application domain.

In this work, we focus on determining the structural, electronic, and optical properties of BAs, InAs compounds, and their ternary $B_xIn_{1-x}As$ alloys, using a full-potential linearized augmented plan-wave method (FP-LAPW). The behavior of these materials under hydrostatic pressure has also been studied in a pressure range from 0 to 25 GPa.

2. METHOD OF CALCULATION

In this contribution, we have used the density functional theory (DFT) via a full-potential linear augmented plane wave implemented in WIEN2k code [10], to calculate the structural and electronic properties of $B_xIn_{1-x}As$. About the exchange-correlation energy, we have employed the generalized approximation (GGA) of Perdew–Burke–Enzerhof (PBE98) and the local density approximation (LDA) for structural properties. In addition to these two approximations, the modified Becke–Johnson approximation has been applied for electronic properties. The space is divided into two regions, an interstitial region (IR) and

Table 1. Lattice constants a, bulk modulus B, and pressure derivative of bulk modulus B' for InAs, BAs compounds and ZB $B_xIn_{1-x}As$ alloys

Composition	Value	This work		Other theoretical studies	Experimental data
		GGA	LDA		
InAs	a, Å	6.15	6.02	6.0209[a]	6.0583[a], 6.036[b]
	B, GPa	49.90	59.34	58[c]	–
	B', GPa	4.07	4.76	4.79[d]	–
$B_{0.25}In_{0.75}As$	a, Å	5.93	5.92	–	–
	B, GPa	58.10	67.89	–	–
	B', GPa	4.25	4.90	–	–
$B_{0.5}In_{0.5}As$	a, Å	5.66	5.56	–	–
	B, GPa	69.83	77.85	–	–
	B', GPa	4.44	4.73	–	–
$B_{0.75}In_{0.25}Asa$	a, Å	5.29	5.21	–	–
	B, GPa	93.80	101.27	–	–
	B', GPa	5.22	4.71	–	–
BAs	a, Å	4.83	4.76	4.72[e]–4.81[f]–4.77[g]	4.77[h]
	B, GPa	135.04	150.23	133f[d]–131[i]–148[e]–145[j]	–
	B', GPa	4.30	3.93	4.29[k], 4.53[k]	–

[a] [12], [b] [13], [c] [14], [d] [15], [e] [1], [f] [16], [g] [17], [h] [18], [i] [2], [j] [19], [k] [20].

a muffin tin region centered at the atomic sites. In the first region, the basis sets consists of plane waves. In the second one, the basis sets are described by radial solutions of the one particle Schrödinger equation. For the matrix size, we used a parameter $R_{MT}K_{max} = 7$, where R_{MT} denotes the minimum radius of the sphere muffin tin in unit cell, and K_{max} gives the magnitude of the largest K vector in the plane wave expansion. The muffin tin radii of B, In, and As are chosen to be 1.45, 2.1, and 2 Bohr radius, respectively.

3. RESULTS AND DISCUSSIONS

3.1. Structural Properties

Firstly, we start by optimizing the cohesive energy of our binary compounds (BAs and InAs) and their ternary alloys $B_xIn_{1-x}As$ in zinc-blende (ZB) structure with GGA and LDA approximations. Our compound have been modeled for the concentrations x = 0, 0.25, 0.5, 0.75, 1 with periodically repeated supercells of eight atoms per unit cell.

We explored the structural optimization by minimizing the total energy with respect to the parameters and the atomic positions, in order to obtain the equilibrium lattice parameter and the bulk modulus for the binary compounds and our ternary alloys.

The total energy E_T, given by our calculation, as a function of unit cell volume was fitted by Murnaghan's equation of state [11]:

$$E_T(V) = \frac{B_0 V}{B_0'}\left[\frac{\left(\frac{V_0}{V}\right)^{B_0'}}{B_0' - 1} + 1\right] + E_0 - \frac{V_0 B_0}{B_0' - 1}. \qquad (1)$$

The results compared with other available experimental and theoretical works are cited in Table 1. Our GGA results of binary are in best agreement with values given in [12–20].

Figure 1 shows the variation of the calculated equilibrium lattice parameter as a function of concentration x for $B_xIn_{1-x}As$ alloys, which indicates a small deviation from Vegard's law with an upward bowing parameter equal to 1.344 Å for the GGA approximation and 1.312 Å for the LDA one.

The bowing parameter is determined by fitting the calculated values with a polynomial function. The important difference between the lattice parameters of our binary compounds (BAs and InAs) is at the origin of such deviation.

In Fig. 2 that indicates the composition dependence of the bulk modulus of $B_xIn_{1-x}As$ alloys, the

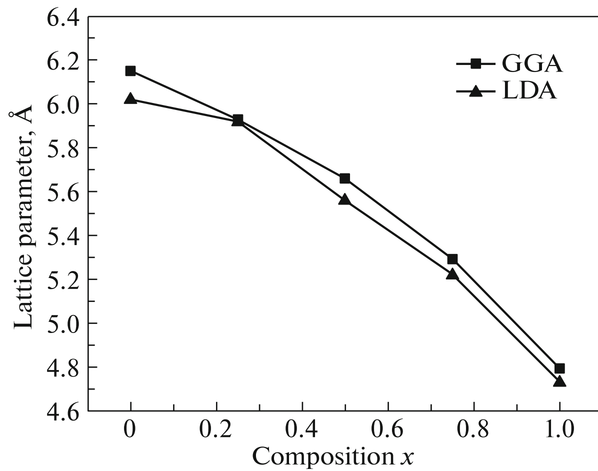

Fig. 1. Composition dependence of the calculated lattice constants of ZB $B_xIn_{1-x}As$ alloys.

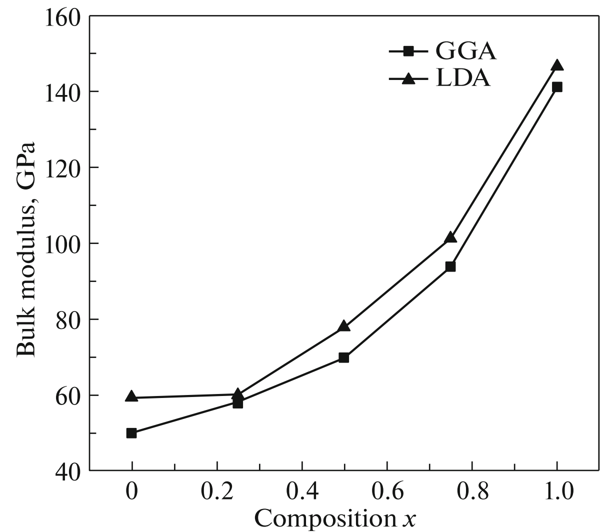

Fig. 2. Composition dependence of the calculated bulk modulus of ZB $B_xIn_{1-x}As$ alloys.

values of the bulk modulus increase with the boron concentration, meaning that the addition of boron to InAs improves their hardness in good agreement with others works.

For this parameter, we can remark a considerable deviation from LCD (linear composition dependence) with downward bowing equal to −16.2777 and −22.605 GPa with GGA and LDA, respectively. The important bowing values are also mainly due to the significant mismatch of the bulk modulus of BAs and InAs.

3.2. Electronic Properties

3.2.1. Band structure. We have performed a first-principle calculation for electronic properties, in order to study the electronic band structure of our binary compounds (InAs and BAs) and their ternary alloys ($B_xIn_{1-x}As$) in ZB structure. We have used the generalized gradient and the modified Becke–Johnson approximations using in full-potential linearized augmented plane wave (FP-LAPW) implemented in WIEN2k code, with the aim to know more opportunity to improve the electronic characteristics of optoelectronic devices using this category of materials and extend their applications fields. It should be noted that we have found difficulties to compare our results with few works in the literature devoted to study the electronic properties of this class of materials [1, 10, 12, 21].

After full optimization and the calculation of the structural parameters, the electronic band structures computed along some high-symmetry directions in the Brillouin zone have been shown in Figs. 3–7.

The zero energy is selected to coincide with the top of valence band, for our studied compounds. We can note that the calculations indicate that the valence band maximum (VBM) is located at Γ point and the conduction band minimum (CBM) at Γ point for $x = 0$, at R point for $x = 0.75$, and at X point for $x = 1$, which means a direct gap semiconductor for InAs, and

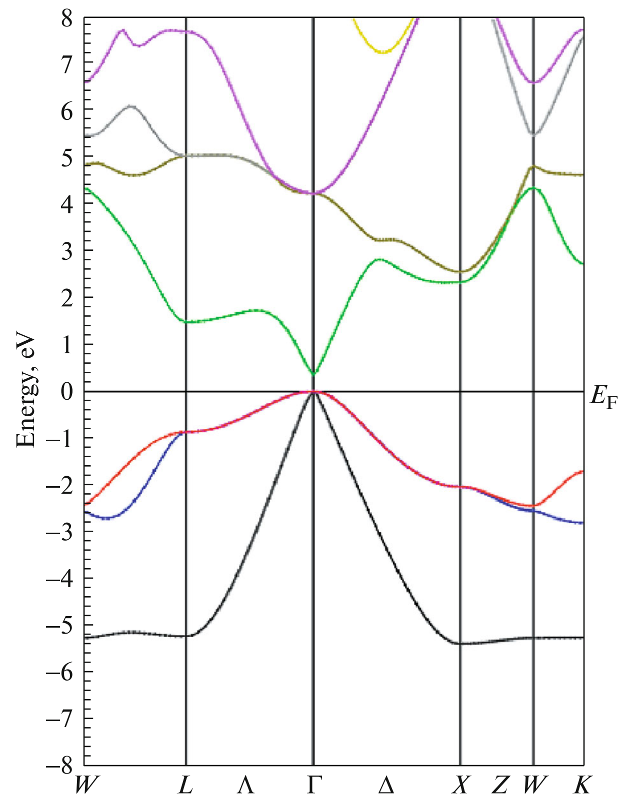

Fig. 3. Non-relativistic mBJ band structure of ZB InAs compound.

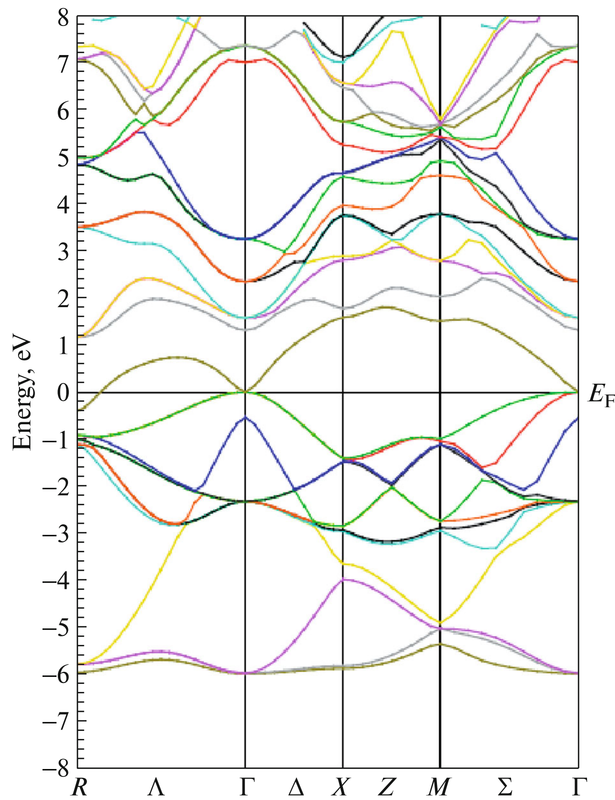

Fig. 4. Non-relativistic mBJ band structure of ZB $B_{0.25}In_{0.75}As$.

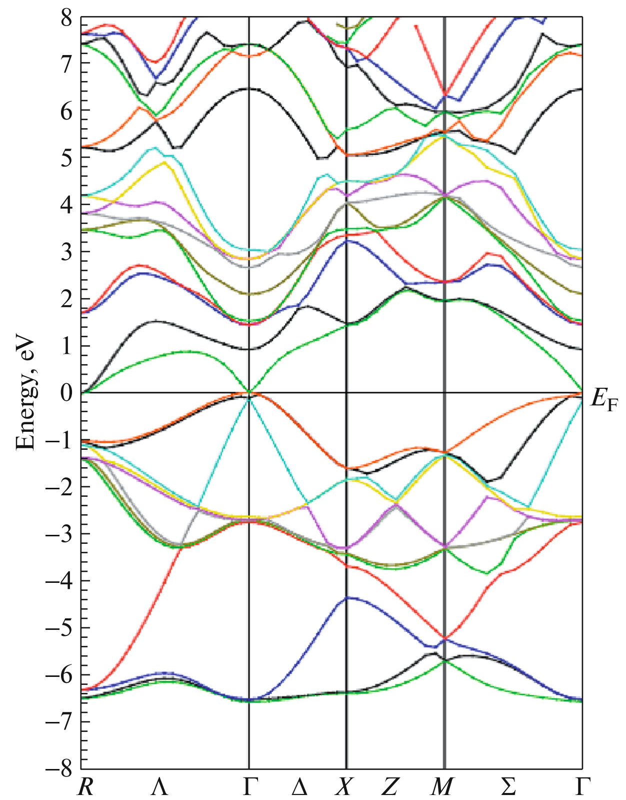

Fig. 5. Non-relativistic mBJ band structure of ZB $B_{0.5}In_{0.5}As$.

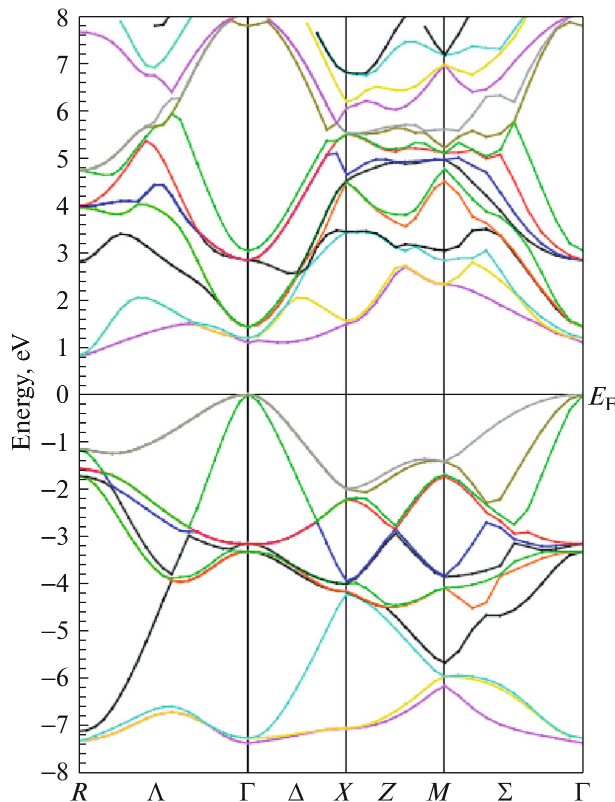

Fig. 6. Non-relativistic mBJ band structure of ZB $B_{0.75}In_{0.25}As$.

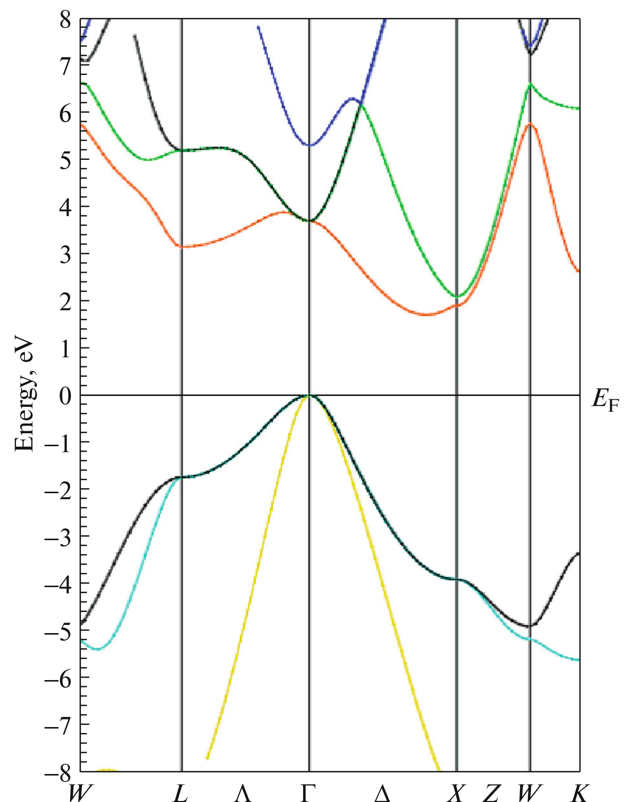

Fig. 7. Non-relativistic mBJ band structure of ZB BAs compound.

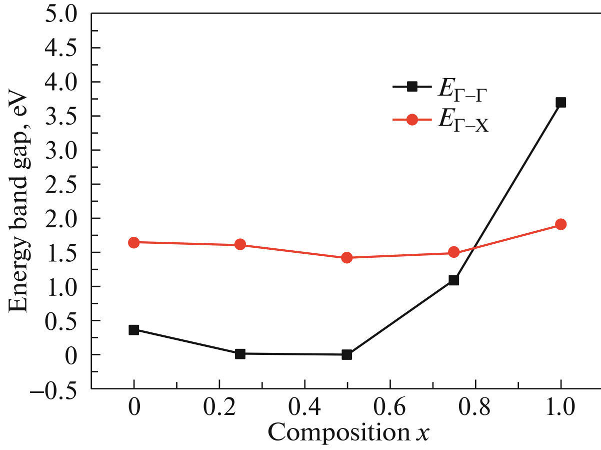

Fig. 8. Composition dependence of the mBJ band gaps for $B_xIn_{1-x}As$ alloys.

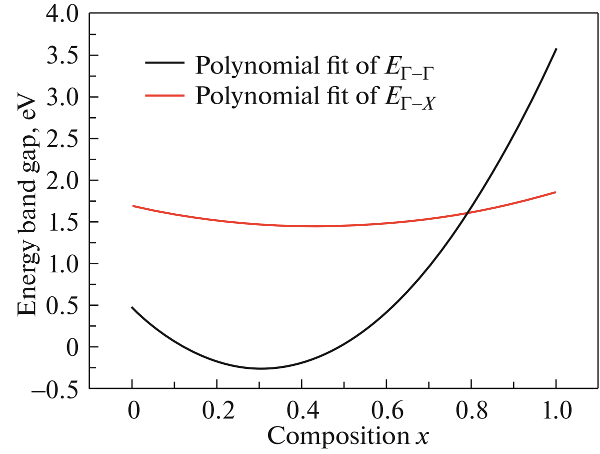

Fig. 9. Composition dependence of the fitted mBJ band gaps for $B_xIn_{1-x}As$ alloys.

an indirect gap semiconductor for BAs in good agreement with [22] in the direction Γ–X, and an indirect gap semiconductor for $B_{0.75}In_{0.25}As$ in the direction Γ–R.

We found that our compound has a metallic and semi-metallic behavior for $B_{0.25}In_{0.75}As$ and $B_{0.50}In_{0.50}As$, respectively. In order to obtain the bowing parameter, we have fitted the non-linear variation of the calculated direct and indirect band gaps in terms of concentration with polynomial function, which obey to the following equations:

$$E_{\Gamma-\Gamma} = 0.476 - 4.843X + 7.955X^2, \quad (2)$$

$$E_{\Gamma-X} = 1.694 - 1.183X + 1.340X^2. \quad (3)$$

Figures 8 and 9 show the variation of the fitted direct and indirect band gaps.

It should be noted that the values of E_g represent a deviation from the linear behavior about 7.95 and 1.34 eV for Γ–Γ and Γ–X band gap, respectively. We can also note that the addition of a weak percentage of boron can significantly increase the width of the gap.

Our computed results compared with the few available data are summarized in Table 2, which indicates a good agreement.

3.2.2. Density of states. By using FP-LAPW method with GGA approximation, we have also calculated the total and partial density of states for BAs, InAs, and $B_{0.75}In_{0.25}As$. The density of states function gives the number of states that are available in a system and is essential for determining the carrier concentrations and energy distributions of carriers, and from this function we can clearly understand the contribution of each atom compared to the total density.

Because the calculations of the density of states request a high degree of precision with use of K-points mesh in the first Brillouin zone. In fact, we used a *k*-mesh of 250 special K-points for $B_{0.75}In_{0.25}As$ ternary alloy and 1000 special K-points for binary BAs and InAs compounds. We have distinguished the B ($1s^2$), In ($1s^22s^22p^63s^23p^63d^{10}4s^24p^6$), and As ($1s^2 2s^22p^63s^23p^6$) inner-shell electrons from valence electrons of B ($2s^22p^1$), In ($4d^{10}5s^25p^1$), and As ($3d^{10}4s^24p^3$) shells.

The spectrum of density of states of the binary BAs, shown in Fig. 10, present three regions, two in valence

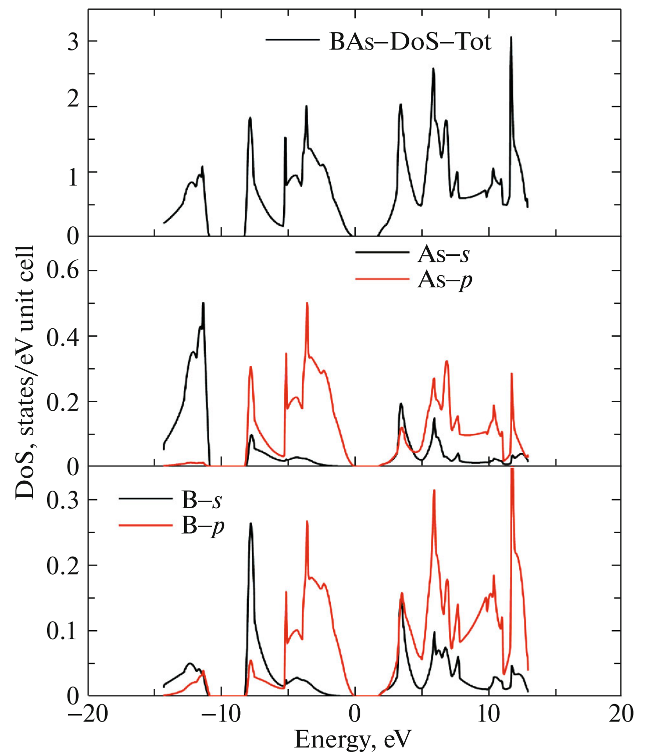

Fig. 10. Total and partial DoS of BAs.

Table 2. Summary of the band gaps of InAs, BAs compounds and ZB $B_xIn_{1-x}As$ alloys

Composition	Energy, eV	This work		Other theoretical studies	Experimental data
		GGA	mBJ		
InAs	$E_{\Gamma-\Gamma}$	0.3812	0.36	0.36[a], 0.40[b], 0.355[c]	0.36[d]
	$E_{\Gamma-X}$	1.658	1.64	1.36[a], 1.37[e]	1.37[d]
$B_{0.25}In_{0.75}As$	$E_{\Gamma-\Gamma}$	00	0.009	–	–
	$E_{\Gamma-X}$	1.57	1.597	–	–
	$E_{\Gamma-R}$	–	–0.3951	–	–
$B_{0.5}In_{0.5}As$	$E_{\Gamma-\Gamma}$	0.139	0	–	–
	$E_{\Gamma-X}$	1.696	1.42	–	1.46[f]
$B_{0.75}In_{0.25}Asa$	$E_{\Gamma-\Gamma}$	1.035	1.13	–	–
	$E_{\Gamma-X}$	1.35	1.47	–	–
	$E_{\Gamma-R}$	–	0.82	–	–
BAs	$E_{\Gamma-\Gamma}$	3.21	3.69	3.34[f], 3.46[g]	1.46[h]
	$E_{\Gamma-X}$	1.41	1.90	1.20[i]–1.46[j] 1.93[e], 1.22[g]	0.67[k]

[a] [21], [b] [4], [c] [22], [d] [24], [e] [25], [f] [23], [g] [1], [h] [26], [i] [27], [j] [16], [k] [28], [l] [29].

region below the Fermi level E_F and one in conduction band (CB) above E_F.

The lower valence band (LVB) is dominated by As-4*s*, the As-4*p* participates in upper valence band (UVB), with a few contribution of B-2*s* and B-2*p*. CB is mainly formed by B-2*s* and As-4*p* with a small contribution of As-3*d*.

For InAs, the DOS spectrum, displayed in Fig. 11, indicates also three main regions, LVB principally dominated by As-4*s* with a few participation of In-4*d*. In-5*s* and In-5*p* contribute in the other valence region.

The third region is formed by a mixture of In-5*p*, As-4*p*, In-4*d*, and As-3*d*.

Our $B_{0.75}In_{0.25}As$ ternary alloy possess a DoS with a similar topography, composed of three region as shown on Fig. 12, with two valence regions (LVB and UVB) below the Fermi level and one in CB above E_F.

From left to right, in the first region (LVB) all the different atoms contribute with a comparable order. The next region (UVB), the orbitals B-2*s*, In-5*s*, and As-4*s* are at the origin of its formation, with a contribution of the orbital *p* of B, In, and As atoms toward the end of this region. In CB, the last region, we have a contribution of all orbitals with a comparable order. We can see that the addition of the boron atom can changed the topography of the different contribution, and at 75% boron concentration, the gap of our alloy increase considerably compared to that of InAs, which means that our alloy can be very useful for various applications in future.

3.3. Optical Properties

To understand the behavior of electrons and ions of our binary compounds and our $B_{0.75}In_{0.25}As$ ternary alloy in interaction with an electromagnetic wave, we will be interested on optical properties. The dielectric function is expressed as $\varepsilon(\omega) = \varepsilon_1(\omega) + i\varepsilon_2(\omega)$, where $\varepsilon_2(\omega)$, the imaginary part, can be calculated from the momentum matrix elements combining the occupied and unoccupied states, which is given by

$$\varepsilon_2(\omega) = \frac{e^2\hbar}{\pi m^2\omega^2}\sum_{v,c}\int_{BZ}|M_{cv}(k)|^2\,\delta[\omega_{cv}(k)-\omega]d^3k. \quad (4)$$

The integral is over the first Brillouin zone. The momentum dipole elements are given as

$$M_{cv}(k) = \langle u_{ck}|\delta\nabla|u_{vk}\rangle, \quad (5)$$

where δ is the potential vector defining the electric field. The $M_{cv}(k)$ are matrix elements for direct transitions between the valence band, $u_{vk}(r)$ and conduction band, $u_{ck}(r)$ states.

Using the Kramers–Kronig relationships, we can deduct the real part $\varepsilon_1(\omega)$ of the dielectric function, which is given by the following formula:

$$\varepsilon_1(\omega) = 1 + \frac{2}{\pi}P\int_0^\infty \frac{\omega'\varepsilon_2(\omega')}{\omega'^2-\omega^2}d\omega', \quad (6)$$

where P implies the principal value of the integral.

Using a FP-LAPW calculation, we can calculate the real and imaginary parts of the frequency-dependent dielectric function, and we can easily deduce the refractive index of our binary compounds BAs and

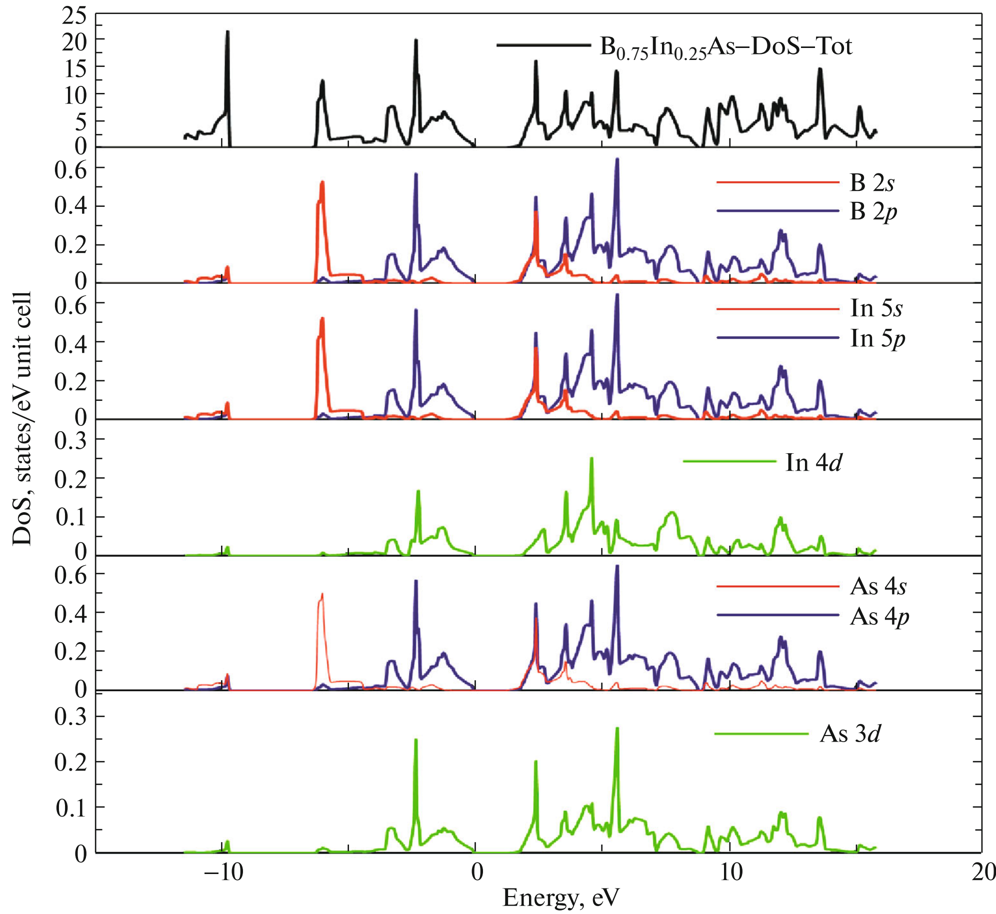

Fig. 11. Total and partial DoS of $B_{0.75}In_{0.25}As$.

InAs and our $B_{0.75}In_{0.25}As$ ternary alloy by using of the following expression:

$$n(\omega) = \left[\frac{\varepsilon_1(\omega)}{2} + \frac{\sqrt{\varepsilon_1^2(\omega) + \varepsilon_2^2(\omega)}}{2}\right]^{1/2}. \quad (7)$$

Figures 13 and 14 show the real and the imaginary parts of the dielectric function as well as refractive index spectrum for a radiation up to 14 eV for binary InAs, BAs compounds and their ternary $B_{0.75}In_{0.25}As$ alloy.

From these figures, we can clearly see that the optical spectrum doesn't vary remarkably.

We can see from Fig. 13, for the real part, that the energy of the main peak in the ultraviolet region shifts toward lowers energy values in the visible regions, from 3.75 eV for BAs to 2.32 eV for $B_{0.75}In_{0.25}As$ to finally reach the value of 1.75 eV for InAs. The origin of this decrease is related to the electronic band structures of the material.

The frequencies, for which $\varepsilon_1(\omega) = 0$, correspond to a maximum of absorption and absence of dispersion, and are located in the ultraviolet region. We noticed a decrease from 5.76 to 4.56 to 4.09 eV for BAs, $B_{0.75}In_{0.25}As$, and InAs, respectively. For higher frequencies corresponding to $\varepsilon_1(\omega) < 0$, the electromagnetic waves don't propagate, and our compounds have an important reflectivity inducing a metallic behavior.

From our calculations results, we can also notice that $\varepsilon_1(0)$ increases from BAs to $B_{0.75}In_{0.25}As$ to InAs, which is due to the fact that the energy gap decreases from BAs to $B_{0.75}In_{0.25}As$ to InAs.

The imaginary part values of the dielectric function based on the photon energy are also shown in Fig. 13. The critical energy point occurs at about 3.11 and 1.51 eV for BAs and $B_{0.75}In_{0.25}As$, respectively. These values correspond to the threshold for direct optical interband transitions at the r point from the top of the valence band to the bottom of the conduction band. In addition, the main peaks are observed at energies of 5.65, 4.18, and 4.15 eV for the BAs, $B_{0.75}In_{0.25}As$, and InAs compounds, respectively.

The refractive index displayed in Fig. 14, which is defined as a dimensionless number, is obtained from

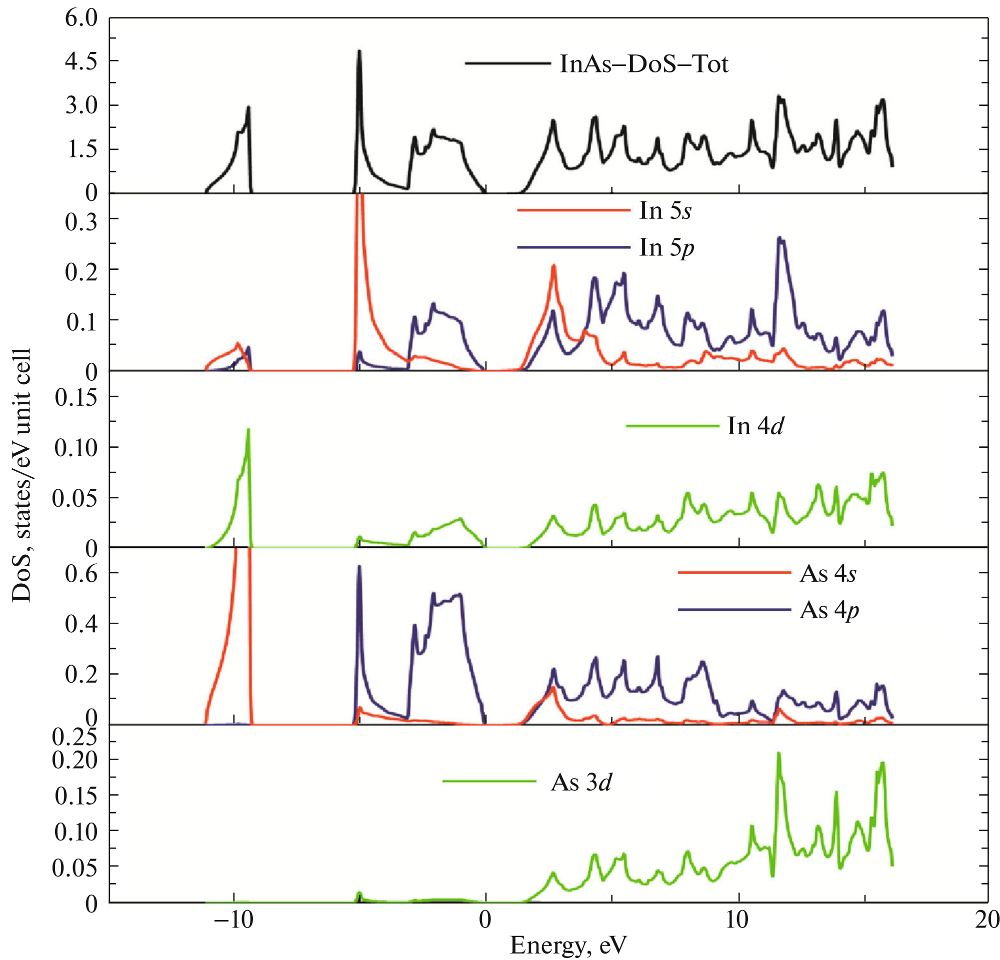

Fig. 12. Total and partial DoS of InAs.

ε_1 and ε_2 values. At the frequency $\omega = 0$, the static refractive index can be obtained using the formula [30]

$$n(0) = \sqrt{\varepsilon_1(0)}. \tag{8}$$

In order to compare our results with others approaches, the refractive index has been also obtained using other empirical models related to the fundamental energy band gap:

(1) Herve and Vandamme's empirical relation [31]:

$$n = \sqrt{1 + \left(\frac{A}{E_{g+B}}\right)} \tag{9}$$

with $A = 13.6$ eV and $B = 3.4$ eV.

(2) The expression proposed by Ravindra et al. [32]:

$$n = \alpha + \beta E_g, \tag{10}$$

where $\alpha = 4.084$ and $\beta = 0.62\ \text{eV}^{-1}$.

In Table 3, the values of the refractive index and the zero-frequency real part, $\varepsilon_1(0)$ of the dielectric function, are given, which can be considered as a measure of the interaction force between the electronic states of the valence and conduction band under an external electric field, of BAs, InAs, and $B_{0.75}In_{0.25}As$ compounds, along with the available experimental and theoretical results.

Our obtained results are in reasonable agreement with other theoretical works. However, for $B_{0.75}In_{0.25}As$ there is no experimental data in the literature for comparison.

For InAs compound, the first peak of the $n(\omega)$ spectrum is located at 1.80 eV with a magnitude of 4.17 and a second major peak is located at around 3.82 eV that corresponds to a magnitude of 3.82, a small peak is also observed at energy of 5.40 eV with a magnitude of 1.92. However, the spectrum of the refractive index increases from its static value at zero frequency, for BAs, until 5.45 eV that corresponds to a magnitude of 4.48. Beyond this energy, the magnitude of refractive index decrease dramatically. For the $B_{0.75}In_{0.25}As$ compound, the refractive index display two minor peaks located at energies of 3.08 and 4.26 eV are

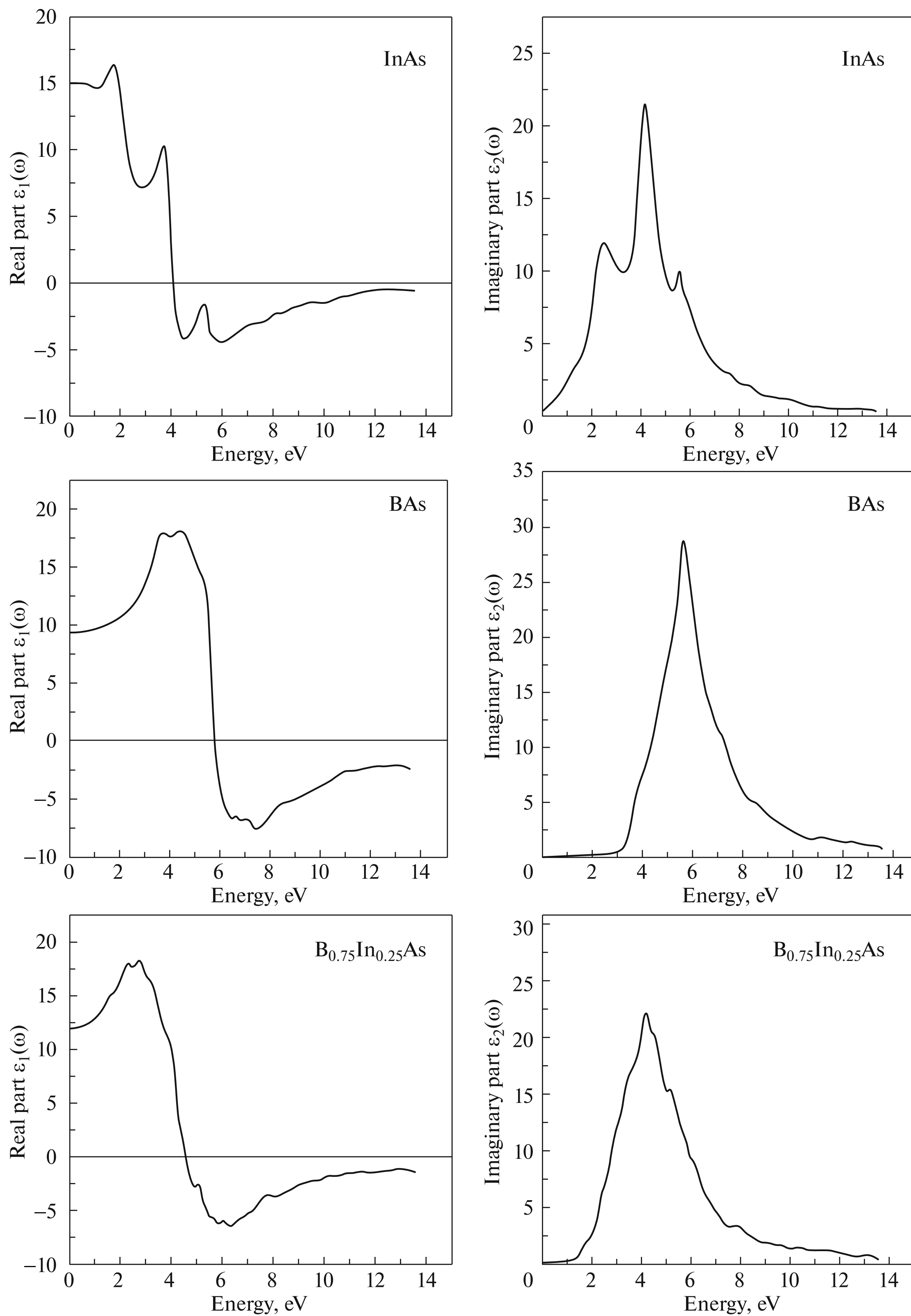

Fig. 13. The real and imaginary parts of the dielectric function of the ZB InAs, BAs, and $B_{0.75}In_{0.25}As$ compounds.

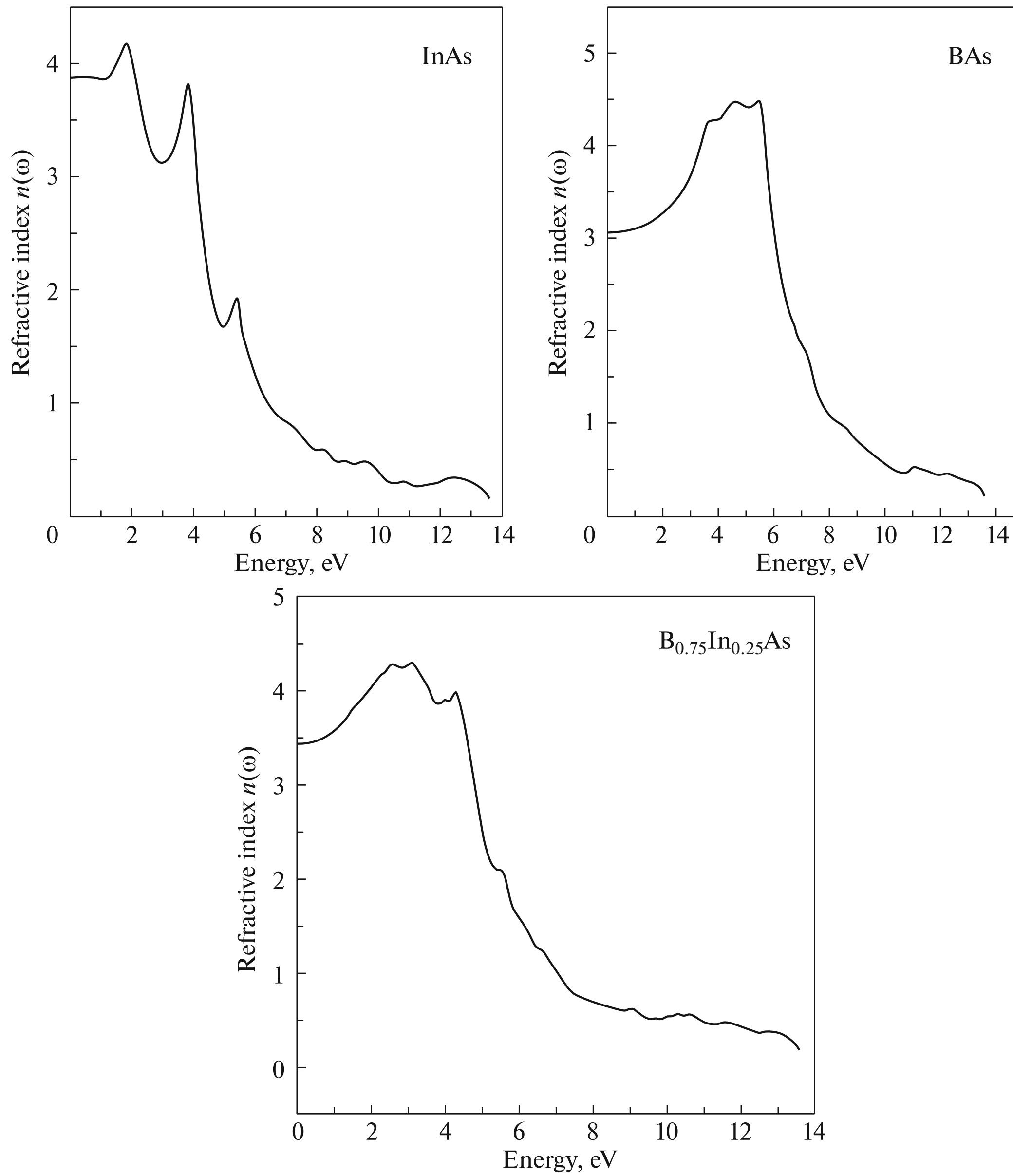

Fig. 14. The refractive index of the ZB InAs, BAs, and $B_{0.75}In_{0.25}As$ compounds.

observed where the corresponding magnitudes are 4.30 and 3.98, respectively.

3.4. Pressure Effect on Electronic and Optical Properties

The arrangement of atoms in a material can be changed under the application of an external perturbation, for example, when we apply hydrostatic pressure to a solid with a given crystal structure, the arrangement of these atoms is modified and probably we pass from a crystalline phase to another. Therefore, the variation of the inter-atomic distance under pressure generally affects its behavior in relation to these electronic properties, structural phase transitions and optical characteristics, etc.

We have studied the effects of pressure on the properties of our binary compound and their ternary alloys using the FP-LAPW method within the WC-GGA and mBJ-GGA approaches and varying the pressure from 0 to 25 GPa with a step size of 5 GPa.

The lattice parameter can be expressed from the relationship given by [39]:

$$a(P) = a(0)\left[1+\left(\frac{B'}{B}\right)P\right], \tag{11}$$

Table 3. Calculated refractive index and dielectric constant for ZB $B_{0.75}In_{0.25}As$, BAs and InAs. Available experimental and theoretical data from the literature are also included for comparison

Composition	Value	This work			Other theoretical studies
		FP-LAPW	relation (9)	relation (10)	
InAs	n	3.88	3.75	4.31	4.09[a], 3.75[b], 3.2[c]
	ε	15.02	14.06	18.58	11.26[d]
$B_{0.75}In_{0.25}$Asa	n	3.44	3.19	4.76	–
	ε	11.96	10.17	22.65	–
BAs	n	3.07	2.75	5.26	3.35[e], 3.12[f]
	ε	9.38	7.56	27.67	9.74[f]

[a] [33], [b] [34], [c] [35], [d] [36], [e] [37], [f] [38].

Table 4. The direct and indirect band gap energies of ZB $B_{0.75}In_{0.25}As$, BAs, and InAs compounds at different pressure values

Composition x at P atom	Band gap energy, eV	Hydrostatic pressure P, GPa					
		0	5	10	15	20	25
BAs	$E_{\Gamma-\Gamma}$	3.69	3.32	3.36	3.39	3.42	3.45
	$E_{\Gamma-X}$	1.90	1.40	1.36	1.33	1.30	1.27
$B_{0.75}In_{0.25}As$	$E_{\Gamma-\Gamma}$	1.13	1.11	1.09	1.04	1.00	0.96
	$E_{\Gamma-X}$	1.47	1.42	1.37	1.33	1.29	1.26
InAs	$E_{\Gamma-\Gamma}$	0.36	0.00	0.16	0.37	0.55	0.70
	$E_{\Gamma-X}$	1.64	1.54	1.45	1.36	1.29	1.23

where B is the bulk modulus, B' is the pressure derivative of the bulk modulus, and $a(P)$ is the lattice parameter at pressure P.

Using the same method, we have also calculated the band gap energies and the results of direct and indirect gaps for each compound under pressure which are shown in Figs. 15a, 15b, and 15c.

From these figures, we can see that the band gap energies $E_{\Gamma-X}$ decrease by increasing the applied pressure. However, concerning the $E_{\Gamma-\Gamma}$ direct gap, our three alloys have a different behavior under the effect of pressure; the gap direct of $B_{0.75}In_{0.25}As$ ternary rapidly decreases under the applied pressure. On the other hand, the value of direct gap of BAs compound decreases in the pressure range from 0 to 5 GPa and then it slowly increases when the applied pressure increases. Furthermore, the direct gap of our InAs binary equals zero at 5 GPa, and therefore it will have a behavior of a semi-metal material (E_g = 0 eV); beyond this pressure, it increases to reach 0.70 eV at 25 GPa.

The first important result is that the applying of a pressure in the range of 0–5 GPa significantly reduced the direct gap of InAs. Consequently, it changes its behavior and it has a semi-metallic behavior. Secondly, our semiconductor alloy $B_{0.75}In_{0.25}As$ remains a direct band gap semiconductor under the range considered for pressure, where the value of its gap decreases with increasing applied pressure.

In Table 4, we summarize the calculated values of the direct and indirect gaps of our BAs and InAs binary compounds and $B_{0.75}In_{0.25}As$ ternary alloys under hydrostatic pressure in the interval from 0 to 25 GPa.

The pressure dependence of the principal band gap energies is given by the empirical formula [39]

$$E_g(P) = E_g(0) + \alpha P + \beta P^2, \qquad (12)$$

where $E_g(0)$ is the band gap energy at zero pressure, α and β are the first- and second-order pressure coefficients, respectively.

Using a non-linear quadratic function, we fitted the results of the direct and indirect band gap of our BAs and InAs binary compounds and $B_{0.75}In_{0.25}As$ ternary alloys.

The quadratic functions for fitting the band gap energies, for each compound, are given as follows:

$$\text{–For } x = 0, \text{ InAs: } \begin{cases} E_{\Gamma-\Gamma} = 0.36 - 0.041P + 0.00213P^2, & (13) \\ E_{\Gamma-X} = 1.64 - 0.021P + 0.00019P^2 & (14) \end{cases}$$

$$\text{–For } x = 0.75, \text{ } B_{0.75}In_{0.25}As\text{: } \begin{cases} E_{\Gamma-\Gamma} = 1.1373 - 0.0045P - 0.0001P^2, & (15) \\ E_{\Gamma-X} = 1.4706 - 0.0105P + 8.5285P^2 & (16) \end{cases}$$

$$\text{–For } x = 1, \text{ BAs: } \begin{cases} E_{\Gamma-\Gamma} = 3.69 - 0.05P - 0.0017P^2, & (17) \\ E_{\Gamma-X} = 1.9 - 0.074P - 0.0020P^2. & (18) \end{cases}$$

In order to study the effect of pressure on the optical properties, in particular on the dielectric function and the refractive index, we also used the same method FP-LAPW. For the different concentrations x, we varied the lattice parameter which is also a function of the applied pressure. Figure 16 shows the cal-

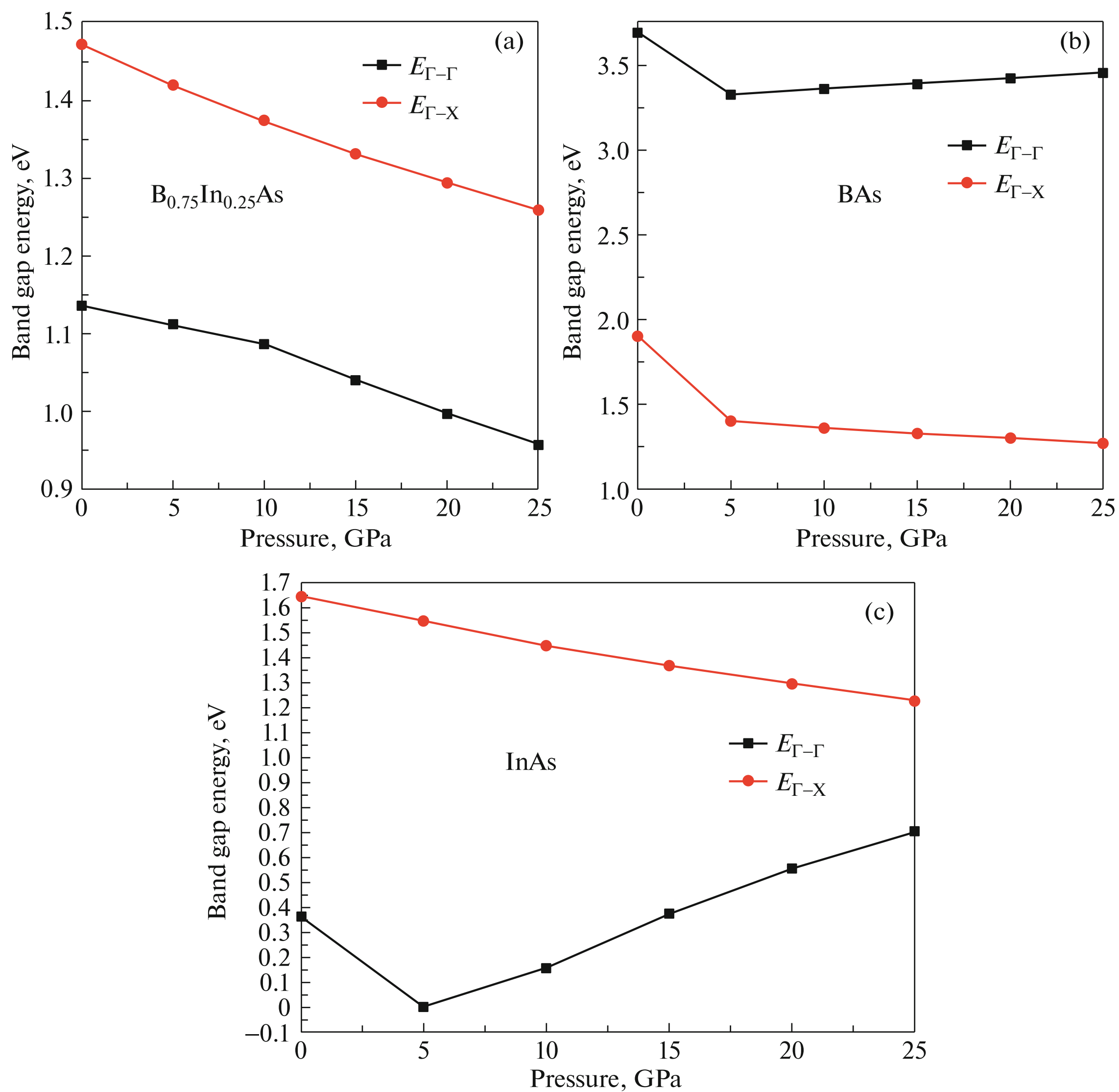

Fig. 15. The direct and indirect band gaps energies versus pressure of the $B_xIn_{1-x}As$ alloy compound at concentrations (a) $x = 0$, (b) $x = 1.00$, and (c) $x = 0.75$.

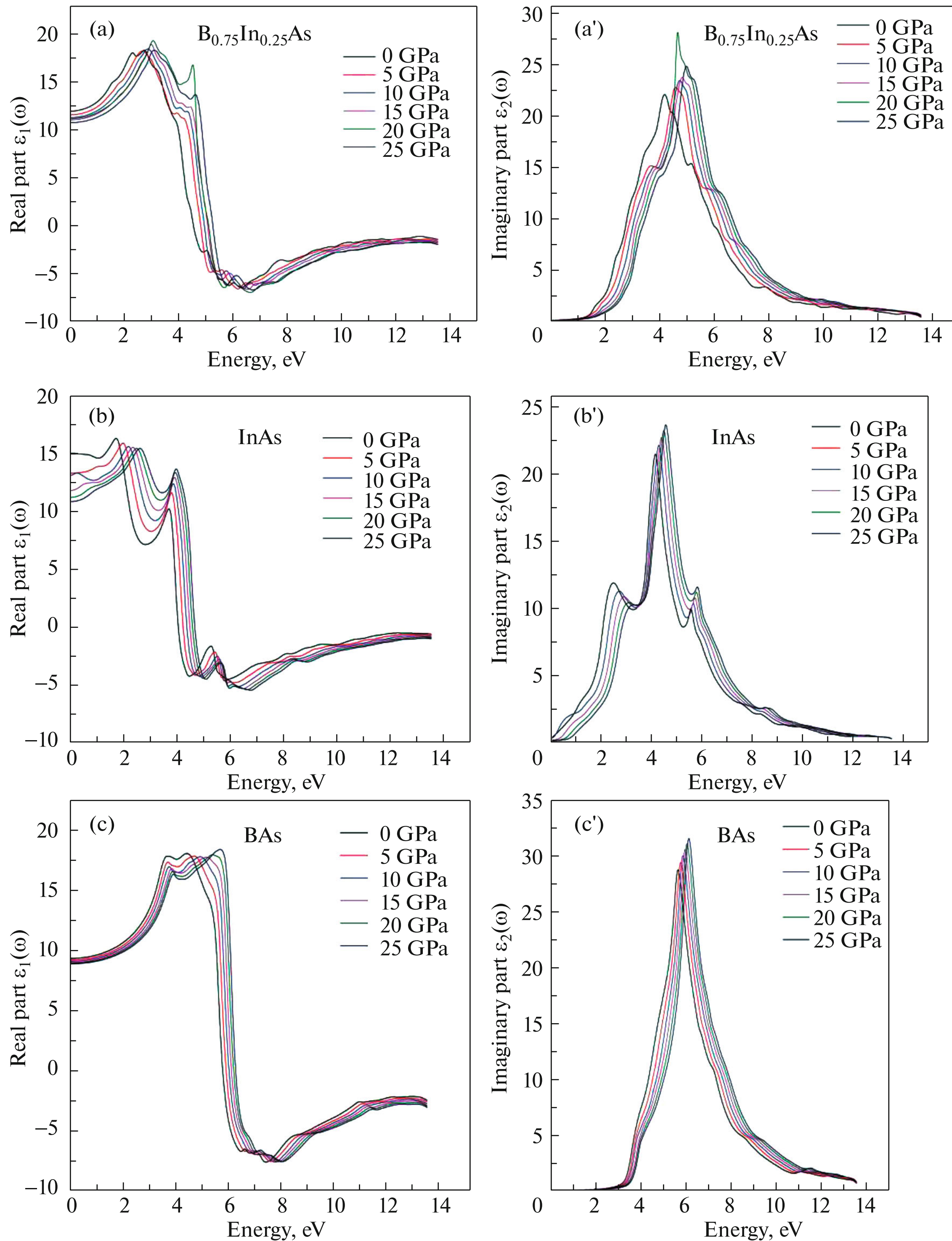

Fig. 16. The calculated real and imaginary parts of the dielectric function under different values of pressure for the BAs, InAs compounds and $B_{0.75}In_{0.25}As$ alloy.

culated real and imaginary parts of the dielectric function under different values of pressure for the BAs, InAs compounds and $B_{0.75}In_{0.25}As$ alloy.

For the real part $\varepsilon_1(\omega)$, as shown in Figs. 16a, 16b, and 16c, we can clearly notice that the spectra at higher pressures keep similar forms to those at ambient

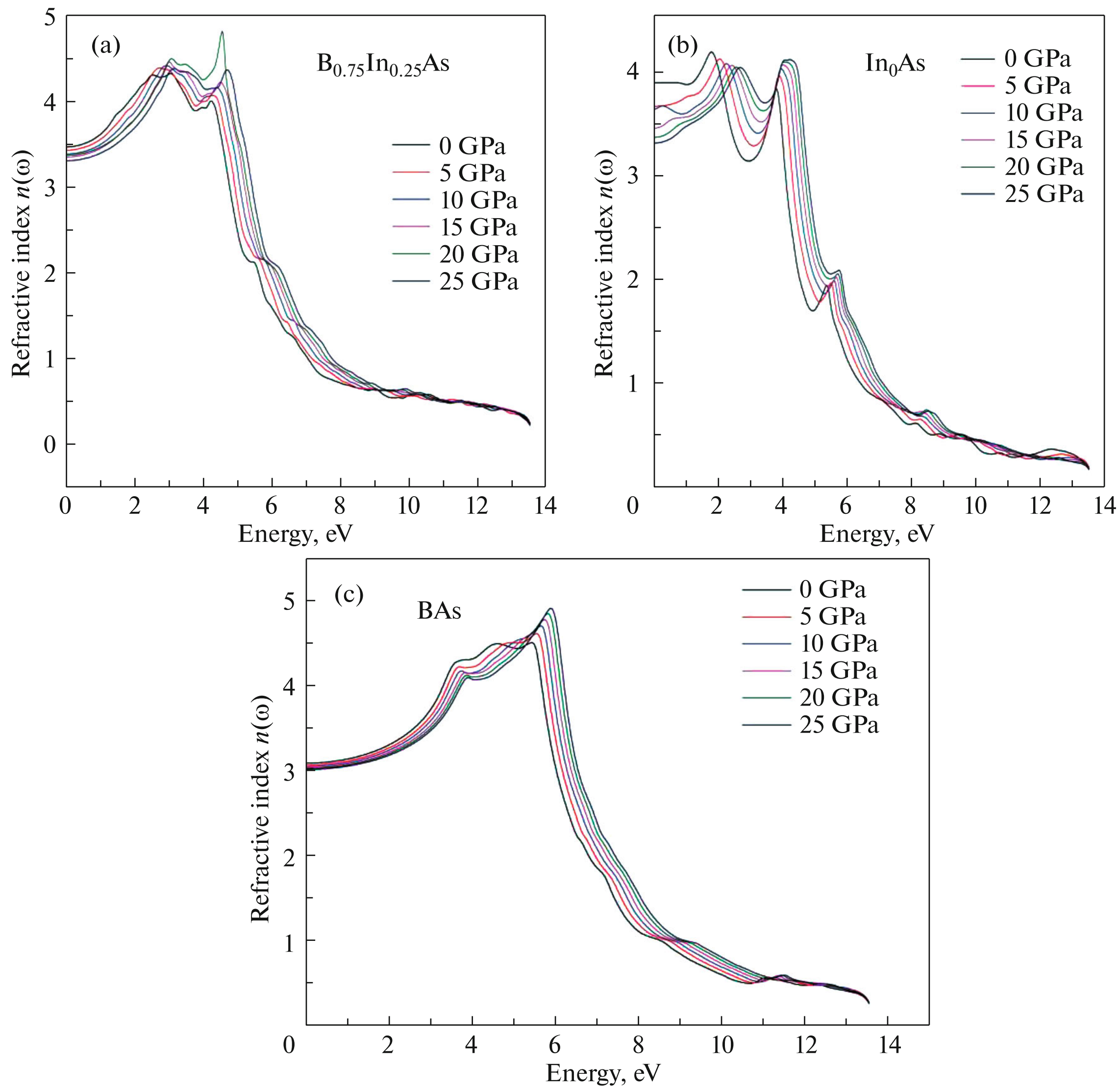

Fig. 17. The calculated refractive index under different values of pressure for the BAs, InAs compounds and $B_{0.75}In_{0.25}As$ alloy.

pressure with a small displacement towards the higher energies when the pressure increases. For $B_{0.75}In_{0.25}As$, we can see the appearance of a small peak for high pressure observed at energy of 4.56 eV.

We can also notice that $\varepsilon_1(0)$ decrease significantly when the pressure applied increases for InAs, which is due to the fact that the energy gap decreases in the same conditions.

For the imaginary parts of the dielectric function, as shown in Figs. 16a', 16b', and 16c', similar forms with a small displacement towards the highest energies when the applied pressure increased was noted, where the amplitude of the spectrum was relatively higher than that with ambient pressure. The energy levels relative to the maximum of the valence band and the minimum of the conduction band under pressure have been displaced, consequently the optical transitions between these energy levels will also be changed, which can be considered at the origin of such changes.

The variation in the refractive index at ambient pressure and under high pressure is also calculated and shown in Fig. 17 spectra that are also of similar forms with the exception of InAs for which there is a remarkable decrease in the static refractive index under pressure; that can be justified by the fact that the pressure considerably affects the band gap energies and affect the optical transitions.

4. CONCLUSIONS

We have presented a FP-LAPW simulation in order to explore structural, electronic, and optical properties of BAs and InAs binary compounds and their $B_xIn_{1-x}As$ ternary alloys under hydrostatic pressure.

Our main results agree very well with other experimental and theoretical data. We can note that the most important results are:

• The incorporation of boron in InAs increases its hardness and affects the band gap energy considerably.

• The addition of low concentration of boron (lower than 25%) reduces the gap, and for the concentrations of more than 50%, the value of the direct gap increases significantly.

• $B_xIn_{1-x}As$ have an indirect band gap for concentration of boron superior to 77%.

• There has been a significant reduction in the gap of InAs in the range from 0 to 5 GPa and it becomes semi-metal at 5 GPa with a decrease in its refractive index in the same range.

• $B_xIn_{1-x}As$ alloy may be an alternative choice for optoelectronic applications at certain concentrations, for example from 0 to 25% of boron at ambient pressure and for 75% under hydrostatic pressure up to 25 GPa.

CONFLICTS OF INTERESTS

The authors declare that they have no conflicts of interest.

REFERENCES

1. N. Chimot, J. Even, H. Folliot, and S. Loualiche, Phys. B (Amsterdam, Neth.) **364**, 263 (2005).
2. F. El Haj Hassan and H. Akbarzadeh, Mater. Sci. Eng. B **121**, 171 (2005).
3. M. Guemou, B. Bouhafs, A. Abdiche, R. Khenata, Y. Al Douri, and S. Bin Omran, Phys. B (Amsterdam, Neth.) **407**, 1292 (2012).
4. R. Ahmed, S. J. Hashemifar, H. Akbarzadeh, M. Ahmed, and F. Aleem, Comput. Mater. Sci. **39**, 580 (2007).
5. M. Ferhat, A. Zaoui, M. Certier, and H. Aourag, Phys. B (Amsterdam, Neth.) **252**, 229 (1998).
6. R. Bhat, P. S. Dutta, and S. Guha, J. Cryst. Growth **310**, 1910 (2008).
7. V. N. Brudnyi, N. G. Kolin, and A. I. Potapov, Semiconductors **37**, 390 (2003).
8. J. A. Perri, S. Laplaca, and B. Post, Acta Crystallogr. **11**, 310 (1958).
9. T. L. Chu and A. E. Hyslop, J. Appl. Phys. **43**, 276 (1972).
10. P. Blaha, K. Schwarz, G. K. H. Madsen, D. Kvasnicka, and J. Luitz, *WIEN2k, An Augmented Plane Wave Plus Local Orbital Program for Calculating Crystal Properties* (Vienna Univ. Technol., Vienna, Austria, 2001).
11. F. D. Murnaghan, Proc. Natl. Acad. Sci. U. S. A. **30**, 244 (1947).
12. Y. Yan, Q. Wang, W. Shu, Z. Jia, X. Ren, X. Zhang, and Y. Huang, Phys. B (Amsterdam, Neth.) **407**, 4570 (2012).
13. R. W. G. Wyckoff, *Crystal Structures*, 2nd ed. (Krieger, Malabar, 1986).
14. K. H. Hellwege and O. Madelung, *Landolt–Börnstein, New Series, Group III* (Springer, Berlin, 1982), Vol. 17, Pt. A.
15. M. Vubcevich, Phys. Status Solidi B **54**, 219 (1972).
16. H. Meradji, S. Labidi, S. Ghemid, S. Drablia, and B. Bouhafs, Phys. Proc. **2**, 933 (2009).
17. H. Bross and R. Bader, Phys. Status Solidi B **191**, 369 (1995).
18. O. Madelung, *Landolt-Börnstein, New Series, Group III* (Springer, Berlin, 1982), Vol. 17a.
19. R. Wentzcovitch, M. L. Cohen, and P. K. Lam, Phys. Rev. B **36**, 6058 (1987).
20. M. Briki, M. Abdelouhab, A. Zaoui, and M. Ferhat, Superlatt. Microstruct. **45**, 80 (2009).
21. N. Tayebi, K. Benkabou, and F. Z. Aoumeur-Benkabou, Phys. B (Amsterdam, Neth.) **407**, 2739 (2012).
22. P. P. Paskov, J. Appl. Phys. **81**, 1890 (1997).
23. T. Hofmann, M. Schubert, G. Leibiger, and V. Gottschalch, Appl. Phys. Lett. **90**, 182110 (2007).
24. S. Adachi, J. Appl. Phys. **61**, 4869 (1987).
25. H. Baaziz, Z. Charifi, and N. Bouarissa, Mater. Chem. Phys. **68**, 197 (2001).
26. M. Merabet, D. Rached, R. Khenata, S. Benalia, B. Abidri, N. Bettahar, and S. BinOmran, Phys. B (Amsterdam, Neth.) **406**, 3247 (2011).
27. A. Zaoui and F. El Haj Hassan, J. Phys.: Condens. Matter **13**, 253 (2001).
28. V. M. Daniel'tsev, N. V. Vostokov, Yu. N. Drozdov, M. N. Drozdov, A. V. Murel, D. A. Pryakhin, O. I. Khrykin, and V. I. Shashkin, J. Surf. Invest. **2**, 514 (2008).
29. M. Rabah, B. Abbar, Y. Al-Douri, B. Bouhafs, and B. Sahraoui, Mater. Sci. Eng. B **100**, 163 (2003).
30. F. Tran and P. Blaha, Phys. Rev. Lett. **102**, 226401 (2009).
31. P. J. L. Hervé and L. K. J. Vandamme, J. Appl. Phys. **77**, 5476 (1995).
32. N. M. Ravindra, S. Auluck, and V. K. Srivastava, Phys. Status Solidi B **93**, 155 (1979).
33. D. E. Aspnes and A. A. Studna, Phys. Rev. B **27**, 985 (1983).
34. M. Othman, E. Kasap, and N. Korozlu, J. Alloys Compd. **496**, 230 (2010).
35. N. Amrane and M. Benkraouda. J. Adv. Phys. **13**, 5041 (2017).
36. M. I. Ziane, Z. Bensaad, B. Labdelli, and H. Bennacer, Sens. Transducers **27** (Spec. Iss.), 374 (2014).
37. R. Wentzcovitch, M. L. Cohen, and P. K. Lam, Phys. Rev. B **36**, 6058 (1987).
38. H. Meradji, S. Labidi, S. Ghemid, S. Drablia, and B. Bouhafs, Phys. Proc. **2**, 933 (2009).
39. S. Adachi, *Properties of Group IV, III–V, and II–VI Semiconductors* (Wiley, New York, 2005), Chap. 2.